Science of the Total Environment 584–585 (2017) 145–153

Contents lists available at ScienceDirect

Science of the Total Environment

journal homepage: www.elsevier.com/locate/scitotenv

Identifying anthropogenic anomalies in air, surface and groundwater temperatures in Germany

Susanne A. Benz [a,*], Peter Bayer [b], Philipp Blum [a]

[a] Karlsruhe Institute of Technology (KIT), Institute for Applied Geosciences (AGW), Kaiserstr. 12, 76131 Karlsruhe, Germany
[b] Ingolstadt University of Applied Sciences, Institute of new Energy Systems (InES), Esplanade 10, 85019 Ingolstadt, Germany

HIGHLIGHTS

- Anthropogenic temperature anomalies are quantified in Germany.
- Temperatures in air, surface and groundwater correlate with nighttime lights.
- Groundwater temperature anomalies are most extreme.
- Heat anomalies in air and groundwater are mainly caused by artificial surfaces.
- Surface urban heat islands are observed in settlements with only 5000 inhabitants.

GRAPHICAL ABSTRACT

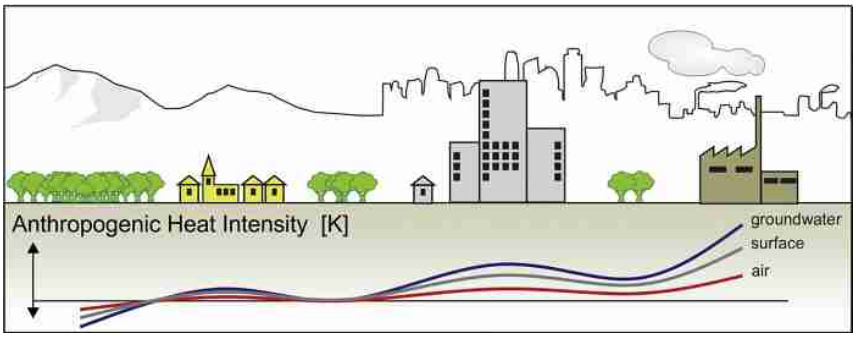

ARTICLE INFO

Article history:
Received 29 November 2016
Received in revised form 20 January 2017
Accepted 20 January 2017
Available online xxxx

Editor: Dr. D. Barcelo

Keywords:
Anthropogenic heat
Surface air temperature
Groundwater temperature
Land surface temperature
Germany
Urban Heat Island

ABSTRACT

Human activity directly influences ambient air, surface and groundwater temperatures. The most prominent phenomenon is the urban heat island effect, which has been investigated particularly in large and densely populated cities. This study explores the anthropogenic impact on the thermal regime not only in selected urban areas, but on a countrywide scale for mean annual temperature datasets in Germany in three different compartments: measured surface air temperature, measured groundwater temperature, and satellite-derived land surface temperature. Taking nighttime lights as an indicator of rural areas, the anthropogenic heat intensity is introduced. It is applicable to each data set and provides the difference between measured local temperature and median rural background temperature. This concept is analogous to the well-established urban heat island intensity, but applicable to each measurement point or pixel of a large, even global, study area. For all three analyzed temperature datasets, anthropogenic heat intensity grows with increasing nighttime lights and declines with increasing vegetation, whereas population density has only minor effects. While surface anthropogenic heat intensity cannot be linked to specific land cover types in the studied resolution (1 km × 1 km) and classification system, both air and groundwater show increased heat intensities for artificial surfaces. Overall, groundwater temperature appears most vulnerable to human activity, albeit the different compartments are partially influenced through unrelated processes; unlike land surface temperature and surface air temperature, groundwater temperatures are elevated in cultivated areas as well. At the surface of Germany, the highest anthropogenic heat intensity with 4.5 K is found at an open-pit lignite mine near Jülich, followed by three large cities (Munich,

* Corresponding author.
E-mail address: susanne.benz@kit.edu (S.A. Benz).

http://dx.doi.org/10.1016/j.scitotenv.2017.01.139

Düsseldorf and Nuremberg) with annual mean anthropogenic heat intensities >4 K. Overall, surface anthropogenic heat intensities >0 K and therefore urban heat islands are observed in communities down to a population of 5000.

1. Introduction

Climate and temperature are strongly affected by humans (IPCC, 2013). The main cause of global climate change is additional greenhouse gas emission that alters the Earth's atmospheric composition (Karl and Trenberth, 2003). However, human activity also affects temperatures on a smaller, local scale. Alterations of surface cover and land use influence the ambient thermal regime (Rhee et al., 2014; Rotem-Mindali et al., 2015; Skinner and Majorowicz, 1999), and, in most cases, cause spatial heat anomalies. These local temperature anomalies are primarily described within the bounds of large urban settlements, where urban temperatures are elevated compared to their rural surrounding and form so-called urban heat islands (UHI) (Hung et al., 2006; Peng et al., 2012). These UHIs have a tremendous impact on human life, energy consumption and the urban ecosystem (Yow, 2007). In France, for example, most consequences of the heat wave in August 2003 occurred in Paris, where an increase of 130% in expected mortality was observed (Dhainaut et al., 2004). Furthermore, the cooling demand of buildings within a city center is approximately 13% higher than in similar buildings in rural areas (Santamouris, 2014). UHIs also change urban phenology: plants tend to develop up to a few weeks earlier in cities compared to their rural surrounding (Jochner and Menzel, 2015). However, with the current research mainly focusing on large city clusters, only little is known about the impact smaller communities and industrial sites have on ambient temperatures (Doyle and Hawkins, 2008; Hinkel et al., 2003) and thus on phenology, energy consumption, and human health.

Urban heat islands can be detected in the atmosphere (Chow and Roth, 2006; Giannopoulou et al., 2011) (e.g. surface air temperature, SAT), at the surface (Pongracz et al., 2010) (land surface temperature, LST) and in the subsurface (Menberg et al., 2013a) (groundwater temperature, GWT). However, the interplay between these different layers is not yet fully understood. A comparison of surface and subsurface UHIs in four German cities showed that, while surface and subsurface temperatures correlate, GWTs are elevated compared to LSTs (Benz et al., 2016). This is due to multiple sources of anthropogenic heat flux into the subsurface, such as the thermal energy release from buildings and reinjection of thermal wastewater (Benz et al., 2015). UHIs in the surface and atmosphere were compared for the city of Leipzig, Germany by Schwarz et al. (2012). They revealed that air temperature and LSTs are related, even so, the UHI in the air was less pronounced.

Urban heat islands are often quantified using the urban heat island intensity (UHII), which is the difference between rural background temperatures and highest urban temperatures (Oke, 1973). A critical component is the rural background temperature, which is not well defined yet and hence differs among presented studies (Martin-Vide et al., 2015; Stewart and Oke, 2012). Both the MODIS Land Cover Product (Peng et al., 2012) and the ASTER land use land cover data (Rajasekar and Weng, 2009) are currently used to differentiate rural areas. Some studies include elevation as an additional parameter for deriving rural background temperatures (Pongracz et al., 2010). In a study by Weber et al. (2014) the distance to the city center was additionally considered. While all of these approaches generally result in an improved understanding of urban heat islands, the variabilities of these results also prevent the comparability. Furthermore, use of non-standard measuring equipment can significantly increase the observed urban heat island magnitudes (Santamouris, 2015) and assessing UHIs becomes rather ambiguous.

The key drivers of urban heat island intensity (UHII) are comprehensively studied (Hoffmann et al., 2012; Menberg et al., 2013b; Ward et al., 2016). However, the results of these studies do not always agree. Oke (1973), for example, found that a cities' atmospheric UHII increases with its population, *P*. In Europe, this dependency is expressed with the following fit: $UHII = 2.10\ K \cdot \log P - 4.06\ K$ ($R^2 = 0.74$). In contrast, Peng et al. (2012) found no evidence of population density driven surface UHII. They also showed only a modest correlation (R^2 of 0.0 to 0.18) between surface UHII and nighttime lights. Only recently though, Zhang et al. (2014) published results indicating a correlation R^2 of 0.83 to 0.85 between summer daytime surface urban heat islands and nighttime light anomalies. Most studies however agree on the effects of vegetation on UHII: within a park or green area, the average temperature difference to the urban surrounding is −0.94 K at the ground level (Bowler et al., 2010).

In this study, the human impact on ambient temperatures is quantified for three different compartments in Germany: air, surface and groundwater. Because above- and below-ground temperatures are influenced differently by seasonal temperature variations (Kurylyk et al., 2014; Smerdon et al., 2006), we chose to analyze annual mean temperatures to ensure comparability. As a universal parameter to quantify anthropogenic heat anomalies, the anthropogenic heat intensity (AHI) is introduced. It is closely related to the UHII, but determined for each pixel (for satellite-derived LST) or measurement point (for SAT and GWT) individually, regardless of land use and location. Hence, it provides the unique and novel opportunity to a) compare the anthropogenic impact on temperatures in air, surface and subsurface, b) to find main instances of anthropogenic temperature anomalies in Germany, and c) to study the impact of smaller settlements or industrial sites on ambient temperatures.

2. Material and methods

2.1. Material

2.1.1. Surface air temperature

Annual mean (2015) surface air temperature (SAT), measured 2 m above ground, was determined in 464 measurement points by taking the arithmetic mean of monthly mean values provided by the German Weather Service (Deutscher Wetter Dienst, DWD, n.d) through their Climate data center (Fig. 1a). SAT is on average 0.26 K colder than land surface temperatures at the same location. The Pearson correlation coefficient between the two is 0.81 (Fig. S1).

2.1.2. Land surface temperature

Annual mean (2015) land surface temperature (LST) was determined from level-5 MODIS daily products MOD11A1 and MYD11A1 (Wan and Dozier, 1996), as obtained from NASA's TERRA and AQUA satellites, courtesy of the NASA Land Processes Distributed Active Archive Center (LP DAAC), USGS/Earth Resources Observation and Science (EROS) Center, Sioux Falls, South Dakota, https://lpdaac.usgs.gov. LST can only be determined for cloud-free days. As Germany has significantly less cloud-cover in summer than in winter, there is more LST data available for this period of the year. Following the approach by Benz (2016), the annual mean was determined from monthly mean temperatures to eliminate this seasonal bias. This calculation was performed in Google Earth Engine, 2015. The results were then exported at a resolution of approximately 1 km × 1 km (0.009° × 0.009°) (Fig. 1b).

2.1.3. Groundwater temperature

Groundwater temperature (GWT) data are only available for the province of Baden-Württemberg in the southwest of Germany. We

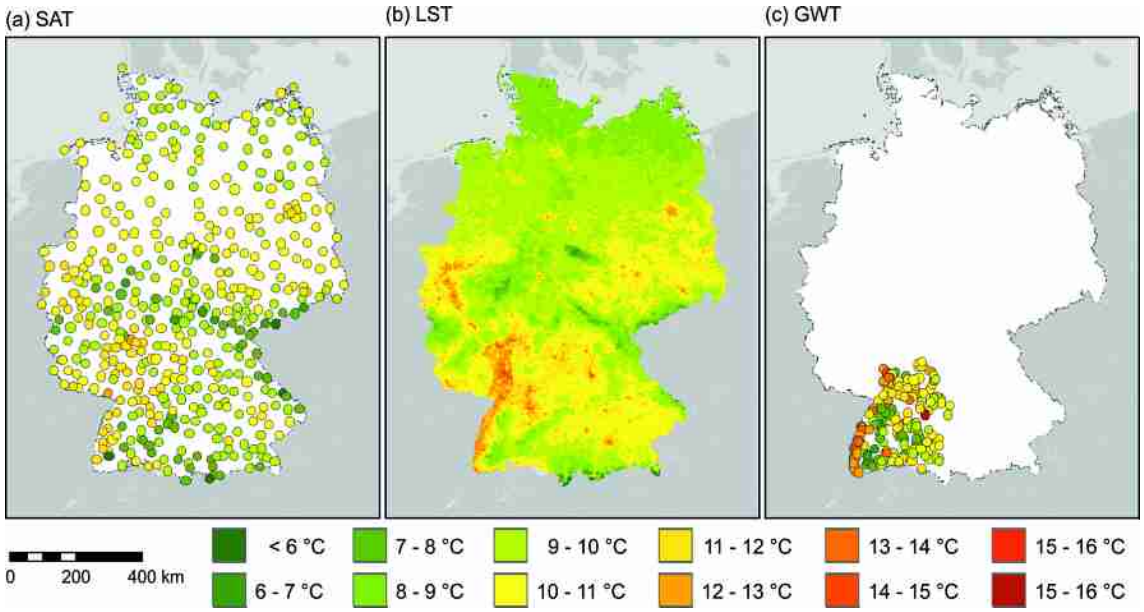

Fig. 1. Mean a) surface air temperature (SAT), b) land surface temperature (LST), and c) shallow (depth ≤ 30 m) groundwater temperature (GWT) of Germany in 2015.

determined annual mean shallow (<30 m depth) GWT in 251 measurement points (MP) for the year 2015 using data provided by the LUBW, 2016 annual catalogue (Fig. 1c and Fig. S2a). To ensure reliable annual mean data for each measurement point, only measurement points with a so-called seasonal radius $r < 0.25$ were used: r is 1.0 if all measurements at the location were conducted in the same month and 0.0 if measurements were uniformly made throughout the year. A seasonal radius that is smaller than 0.25 indicates an unbiased annual mean (Benz et al., 2017). The determined GWTs are on average 0.22 K colder than LST at the same location and the Pearson correlation coefficient is 0.82 (Fig. S1).

2.1.4. Nighttime lights

Nighttime lights were compiled from Version 4 of the DMSP-OLS Nighttime Lights Time Series, Image and Data processing by NOAA's National Geophysical Data Center, and DMSP data collection by the US Air Force Weather Agency. Data were only available up to January 2014, hence 10-year mean (01/2004–12/2013) nighttime lights were chosen. The results were again exported at a resolution of approximately 1 km × 1 km (Fig. 2a) using Google Earth Engine, 2015. For Germany, the spatial median nighttime light is at DN 8 (on a scale from DN 0 to DN 63); a histogram of all data is displayed in Fig. S3. Fig. 2b shows the relationship between nighttime lights and temperatures. LST and nighttime lights correlate and show a Pearson correlation coefficient of 0.55.

2.1.5. Elevation

Fig. 2c is an elevation map of Germany. Elevation data were derived from the Global 30 Arc-Second Elevation (GTOPO30) available from the U.S. Geological Survey and downloaded using Google Earth Engine with a resolution of approximately 1 km × 1 km. Fig. 2d displays the relationship between elevation and temperatures; the moving (±150 m) average LST is given as a black line. The Pearson correlation coefficient between moving average LST and the corresponding elevation is −0.96.

2.1.6. Land cover

Land cover classification for entire Germany was extracted from the GlobCover (2009) Project (Fig. S4). In this study only the three most frequent entries of the land cover classification system (LCCS) are considered: A11 - cultivated terrestrial areas and managed lands; A12 - natural and semi-natural terrestrial vegetation; and B15 - artificial surfaces. Together they cover >98% of the entire analyzed area. Fig. S5 shows the influence of land cover on temperatures. Only minor differences (approximately 0.1 K) in mean LST are observed for the different LCCS entries.

2.1.7. Enhanced vegetation index

The enhanced vegetation index (EVI) is taken from MODIS product Version-5 MYD13A1 by courtesy of the NASA Land Processes Distributed Active Archive Center (LP DAAC), USGS/Earth Resources Observation and Science (EROS) Center, Sioux Falls, South Dakota. The annual mean (2015) EVI was determined in Google Earth Engine, 2015 and exported with a resolution of approximately 1 km × 1 km (Fig. S6a). The Pearson correlation coefficient between LST and EVI is −0.22 (Fig. S6b).

2.1.8. Population data

Population data were provided by the Federal Statistical Office of Germany and represents numbers acquired via a census conducted in 2011. In this study, we used both the spatial distribution of population density provided as a 1 km × 1 km dataset by the census database (Statistisches Bundesamt, Zensusdatenbank, 2011) (Fig. S6c), and the total population of local communities available through Germany's Regional Database (Statistisches Bundesamt, Regionaldatenbank, 2016). No correlation between population density and LST exists (Pearson correlation coefficient: 0.02, Fig. S6d).

2.2. Method

To analyze the anthropogenic influence on temperature, we introduce the anthropogenic heat intensity (AHI). It can be applied to a broad variety of different temperature measurements such as GWT, LST, and SAT. Following the commonly used definition of urban heat island intensity (UHII: max. urban temperature - rural background temperature) (Oke, 1973), AHI is determined by subtracting median rural background temperatures (T_r) from individual temperatures (T) recorded at each measurement point (GWT and SAT) or pixel (LST):

$$AHI = T - median(T_r) \quad (1)$$

While urban land cover and land use classifications are often used to analyze the spatial properties of city-scale urban heat islands (Middel et al., 2014; Stewart et al., 2014), they are not commonly available for such large-scale studies such as this one. Hence, nighttime light was used as

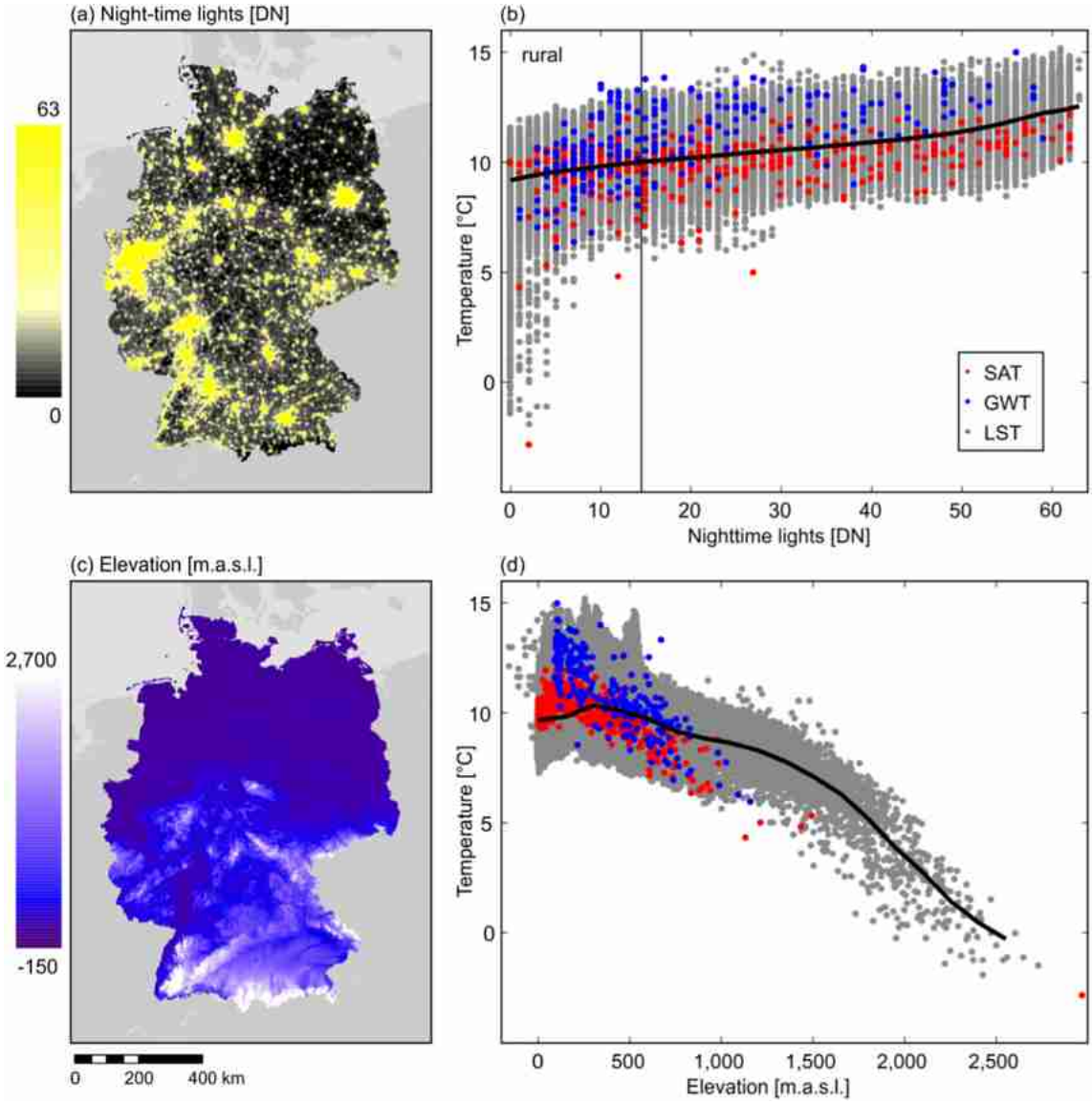

Fig. 2. Influence of anthropogenic nighttime lights and elevation on land surface temperature (LST), surface air temperature (SAT), and groundwater temperature (GWT). The moving average LST is depicted in black in b) and d).

an indicator for rural areas, while elevation and distance to the analyzed pixel or measurement point were considered to find appropriate background measurement locations.

2.2.1. Rural background temperature

Nighttime lights have been intensively discussed as an indicator of urban activity (Imhoff et al., 2010; Li et al., 2016; Mellander et al., 2015). In general, the higher the recorded digital number (DN), the more urban activity is present. This dependency is also visible in the correlation between nighttime lights and temperature (Fig. 2b). To define the area used for the determination of T_r, an upper limit of 'rural' nighttime light has to be set. The method itself is not sensitive regarding the precise value of this upper limit (Fig. S7). The difference in median land surface AHI calculated with an upper limit at DN < 10 and DN < 20 is merely 0.04 K and can therefore be disregarded. Subsequently DN 15 was chosen as the upper limit of allowed nighttime light, because it is both the 75th percentile for nighttime light (Fig. S3) and the first inflection point in the nighttime light – temperature plot (Fig. 2b). Hence, only areas with DN < 15 were considered rural and used to determine T_r. At this number, average LST has increased by 0.8 K from the temperatures at DN 0. In comparison, the difference in average LST between minimal and maximal nighttime lights is 3.4 K.

As temperature decreases significantly with elevation (Fig. 2d), this parameter has to be considered for delineating the background area. As LST increases by 0.8 K from rural nighttime light at DN 0 to DN 15, this value was also chosen as the endorsed change in temperature due to elevation change. Fig. 2d shows the moving (±150 m) average LST. On average, it decreases by 0.004 K/m with a maximal decrease of 0.009 K/m at 1800 m above sea level. Thus, a change in elevation of ±90 m will result in a temperature change of 0.8 K at most. Hence, we only consider data with an elevation ±90 m compared to the analyzed measurement point or pixel.

Variograms of SAT, GWT and LST were set up to determine an appropriate distance between background temperature and analyzed location (Fig. 3). Fitting of the theoretical variograms was performed in MATLAB R2016a using a least square fit with the spherical model, without a nugget. Resulting values for sill and range are shown in Table S1. Since two variograms for LST data (one created from LST at GWT measurement locations and one created from LST at SAT measurement locations) are analyzed, it becomes apparent that sill values depend on the measurement point location. The fitted

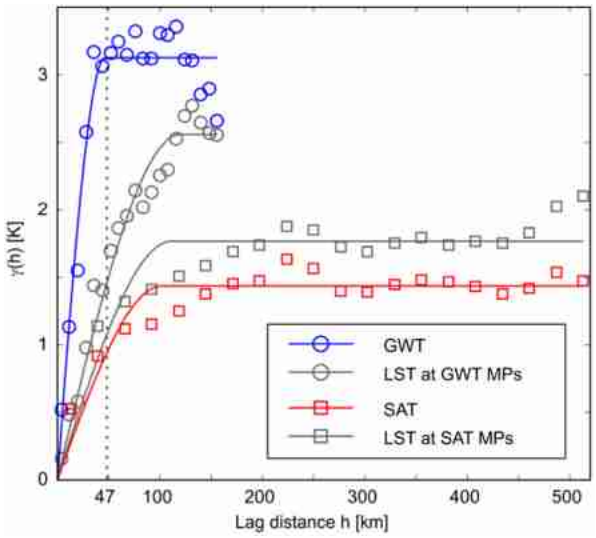

Fig. 3. (Semi-)variogram of all analyzed temperatures. Sill and range are displayed in Table S1. MPs: measurement points.

range, however, is not influenced by measurement point location. It is lowest for GWTs with 47 km. Hence, we chose 47 km as the maximal distance between the analyzed location and the background temperature measurements.

In summary, for the determination of the median rural background temperature T_r of a specific location, only temperature measurements are considered, which a) are within 47 km of the analyzed location, b) have a nighttime light lower than DN 15, and c) are elevated ±90 m compared to the analyzed location. To ensure a statistically meaningful median T_r, AHI was only determined for measurements with five or more rural background measurement points for SAT and GWT, or 50 or more valid rural background pixels for satellite-derived LST.

The introduced method can be applied to any available temperature datasets, from city-scale to global-scale, regardless of the studied compartment (e.g. air, surface or groundwater). To determine whether measurement point location influences the AHI results, we compared surface AHI derived from all pixels with those derived using only data at the GWT and SAT measurement locations (Fig. S8). For both, GWT and SAT measurement points, the RMSE between pixel based and measurement point based AHI is 0.3 K and neglected within this study. Thus, AHIs in different compartments are compared without considering any sampling bias.

3. Results and discussion

Fig. 4 shows the anthropogenic heat intensity (AHI) of Germany in air and surface and the AHI of the province of Baden-Württemberg in groundwater. Results are also made available in the Supplementary material. In the following, we briefly discuss the AHI values in air and groundwater and compare them to surface AHI results. As there is much more LST data (~440,000 pixels) examined than SAT (195 analyzed measurement points) and GWT (186 analyzed measurement points) data, only surface AHI is discussed in detail.

3.1. Air anthropogenic heat intensity

The air AHI ranges from −0.7 K next to a forest in a low mountain range (Swabian Jura) to >1.1 K in three weather stations near Berlin, near Munich, and near the Ruhr city cluster (Fig. 4a, histogram in Fig. S9a). The Pearson correlation coefficient between air and surface AHI is 0.63. The RMSE is 0.5 K and therefore only slightly larger than the expected sampling-location bias of 0.3 K (Fig. 5). Still, the comparison indicates that air temperature shows less anthropogenic warming than surface temperature and therefore confirms the results by Schwarz et al. (2012). However, no definite conclusion can be made with the limited number of measurement points. The influence of land cover on the AHI in the air is displayed in Fig. 6. As expected measurement points in areas classified as 'artificial surfaces' show the highest heat anomaly with a mean air AHI of 0.5 ± 0.5 K (uncertainties are given in form of the standard deviation).

3.2. Groundwater anthropogenic heat intensity

Groundwater AHIs are displayed in Fig. 4c and Fig. S2b, a histogram is given in Fig. S9c. As expected from the high sill and low range in the (semi-)variogram (Fig. 3), AHI in the groundwater has a much broader range than at the surface (Fig. 5). While the RMSE between surface and

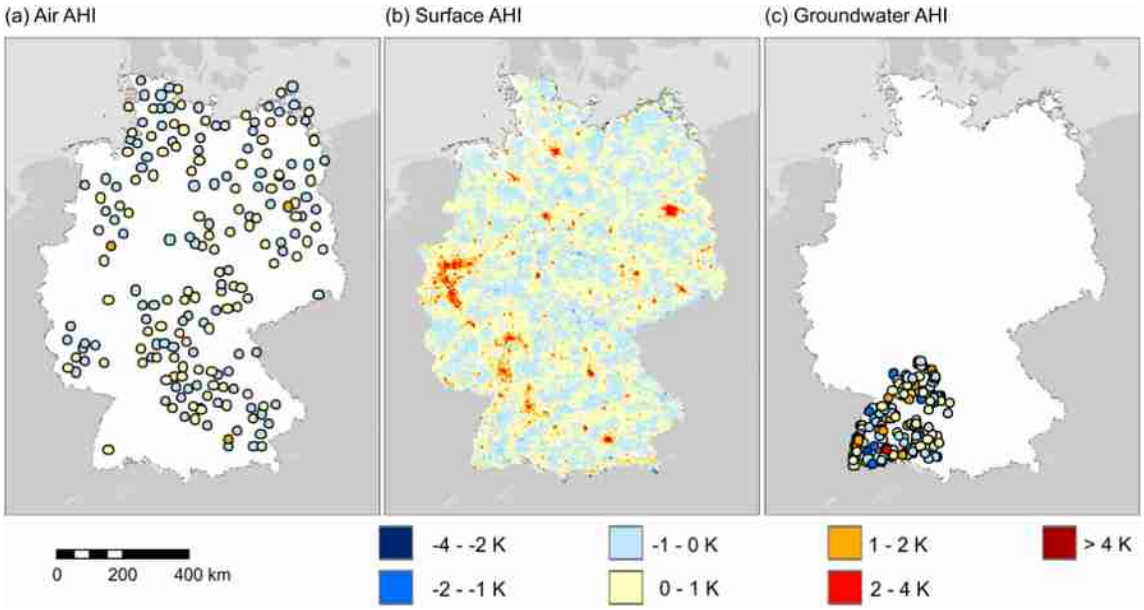

Fig. 4. Anthropogenic heat intensities (AHI) of Germany in (a) air, (b) surface and (c) groundwater.

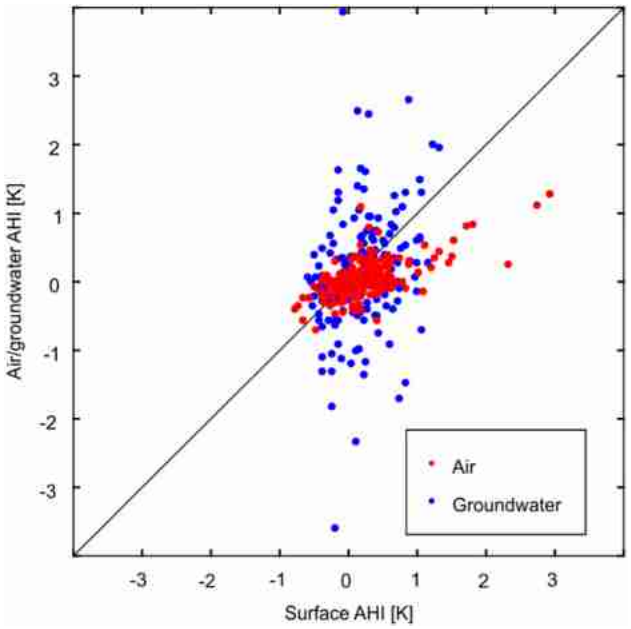

Fig. 5. Comparison of the anthropogenic heat intensities (AHI) of GWT and LST and of SAT and LST.

subsurface AHI is 0.8 K, differences between these two range from −3 to 4 K and both parameters do not correlate (Pearson correlation coefficient: 0.27). Because temperatures themselves correlate well (Fig. S1), this indicates that humans impact groundwater and surface partially through unrelated processes. GWT, for example, is significantly altered by the use of shallow geothermal energy systems such as groundwater heat pumps (Stauffer et al., 2013) as well as reinjection of thermal waste water and subsurface infrastructure such as basements, district heating networks, sewage systems and buried cable systems (Benz et al., 2015; Menberg et al., 2013a; Stegner, 2016).

Fig. 6 shows the influence of land cover on GWT anomalies. Groundwater under artificial surfaces displays the highest anthropogenic heat intensity with a mean value of 2.0 ± 0.7 K. Again, the human impact on temperatures appears to be more prominent in GWT than in LST, verifying previous observations for UHIs (Benz et al., 2016; Perrier et al., 2005). In contrast to SAT and LST, GWTs under cultivated terrestrial areas and managed lands appear to be slightly elevated, on average by 0.2 ± 0.8 K. While the main cause of these anomalies has to be validated yet, they are possibly linked to irrigation with warmer surface water causing advective heat transport into the aquifer.

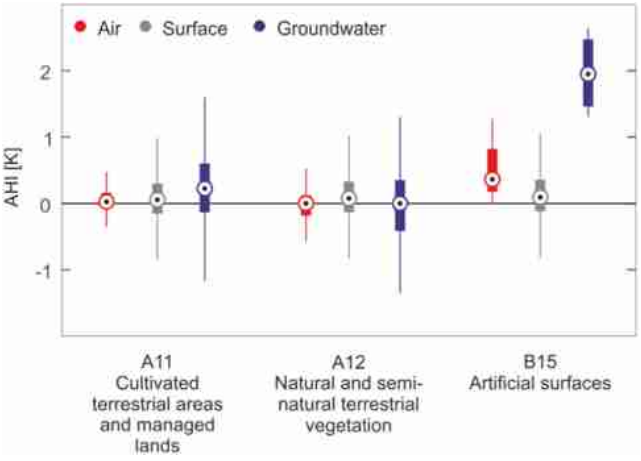

Fig. 6. Influence of land cover on the anthropogenic heat intensity (AHI) in air, surface and groundwater. The dots in the boxplot indicate median values, the bars correspond to the inner quartile range (IQR) ranging from the 25th percentile (P_{25}) to the 75th percentile (P_{75}). Whiskers span from the lowest value higher than $p_{25} - 1.5 \cdot IQR$ to the highest value lower than $p_{75} + 1.5 \cdot IQR$.

3.3. Surface anthropogenic heat intensity

Surface AHI is shown in Fig. 4b. Mean AHI is 0.1 ± 0.5 K; minimum AHI is −4.3 K found in a mountain range of the Northern Limestone Alps within the Berchtesgaden National Park. A histogram is provided in Fig. S9b. The locations of the top 50 maximum surface AHI of Germany are displayed in Table S2. The pixel with the highest annual mean surface AHI (4.5 K) is not found in a city, but over an open-pit lignite mine near Jülich. This extreme temperature anomaly is possibly caused by the immense land cover changes resulting in an open-pit with a depth of approximately 370 m and without vegetation. However, further research is necessary to fully understand temperature anomalies at open pit mines. Pixels with the next highest surface AHIs are located in large cities, namely Munich, Düsseldorf, and Nuremberg, with AHIs of >4 K. The UHI of Munich was studied in1982, when Brundl and Hoppe (1984) determined a 17% higher consumption of heating energy for the outskirts of the city compared to the city center. The surface UHI was quantified by Pongracz et al. (2010). They found an annual mean nighttime UHII of approximately 1.7 K, while daytime UHII spanned from 0 K in December to 5 K in June. These comparably low values are due to the chosen background temperature: A large part of the background area used by Pongrácz et al. (2010) is classified as non-rural in our analysis and therefore not used here.

The top 15 surface AHI locations also include pixels in smaller cities (e.g. Wolfsburg: surface AHI of 3.7 K, 120,000 residents; Saarlouis: surface AHI of 3.4 K, 40,000 residents) known for their industrial sites. This indicates that not only urban heat islands exist, but also industrial heat islands. Furthermore, as our method is applied to all areas including rural ones, we find naturally occurring heat islands as well: there are four locations in the alpine mountains among the top 50 surface AHI locations. Here, the south facing slopes of the high altitude mountain ranges receive more solar radiation and are considerably warmer (>2 K) than the north-facing slopes.

Unlike AHI in groundwater and air, surface AHI cannot solely be linked to artificial surfaces (Fig. 6) using the analyzed classification system (GlobCover, 2009) and resolution (approximately 1 km × 1 km). However, a more detailed case study of the surface UHI of Shanghai revealed differences in temperature of up to 1.6 K between different urban land use and land cover categories (Li et al., 2014).

3.3.1. Main drivers of surface AHI

To determine the main drivers of surface AHI, nighttime lights, elevation, vegetation (enhanced vegetation index, EVI), and population density were analyzed (Fig. 7). Following the trend observed in temperatures (Fig. 2b), AHI rises with increasing nighttime lights (Fig. 7a). The Pearson correlation coefficient ρ between surface AHI and nighttime lights is 0.71. Fig. 7b displays the correlation between elevation and surface AHI (ρ = −0.12). Because our method considers elevation for the determination of the median rural background temperatures, no clear trend is visible in contrast to the temperature/elevation plot (Fig. 2d). However, highest AHI are still observed in lower altitudes, where cities are commonly located. For higher altitudes, AHI variance increases; this is mainly due to the difference in solar radiation on opposite facing slopes of a single mountain range.

In Fig. 7c the enhanced vegetation index (EVI) and surface AHI are compared. While no clear linear correlation is observed (Pearson correlation coefficient: −0.36, Fig. 7c), our results indicate that vegetation decreases the upper limit of surface AHI. This further validates the observations made by several studies on the cooling effect of vegetation

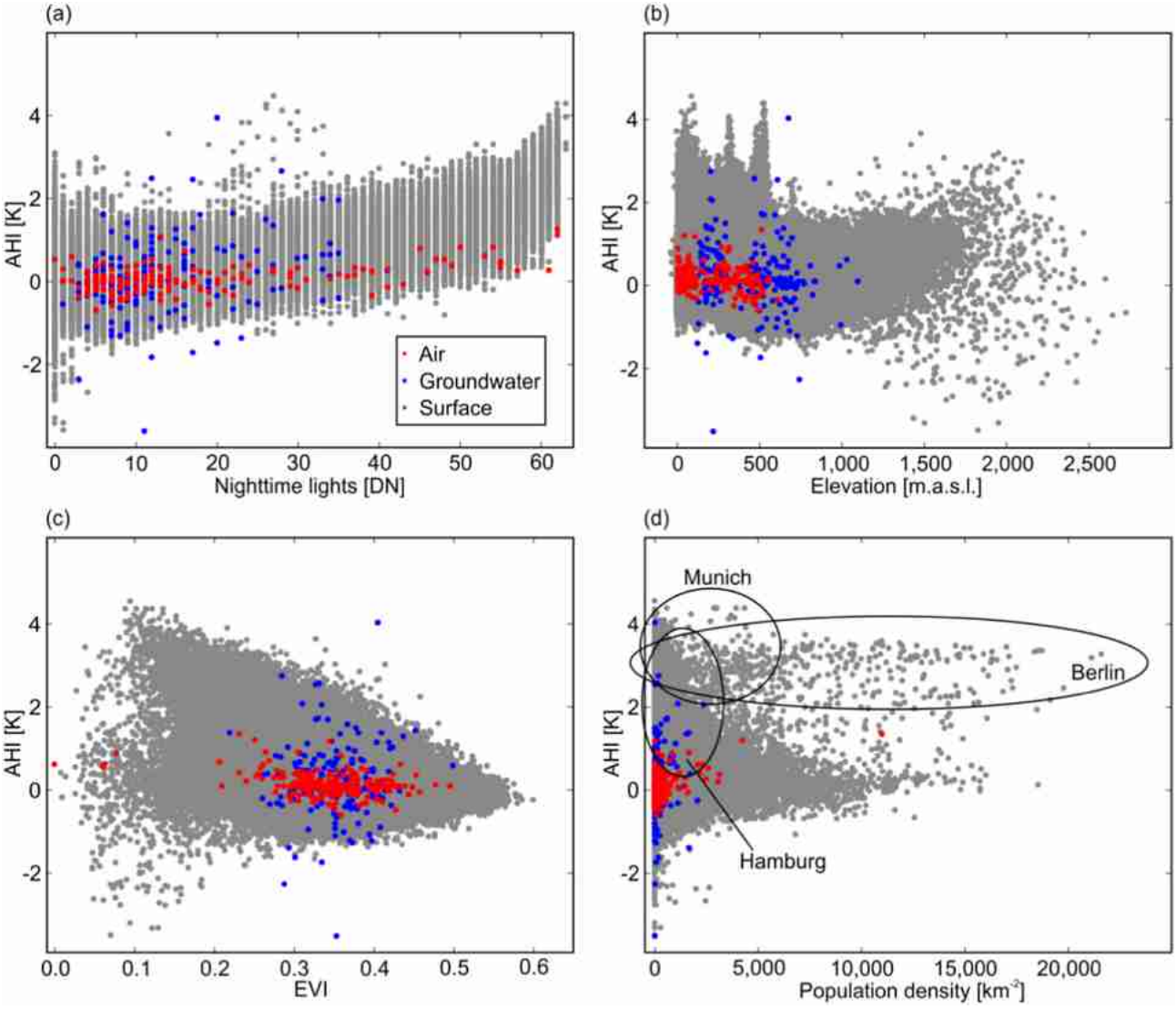

Fig. 7. Influence of nighttime lights, elevation, enhanced vegetation index (EVI), and population density on the anthropogenic heat intensity (AHI) in air, surface and groundwater.

on urban temperatures (Fallmann et al., 2013; Gioia et al., 2014; Zhibin et al., 2014).

Pearson correlation coefficient of 0.06 illustrates that the population density per pixel is no indication for AHI (Fig. 7d). While pixels in large cities such as Berlin (3.3 million residents), Hamburg (1.7 million residents), and Munich (1.3 million residents) show increased AHI, highest heat intensities are not necessarily found in areas with a high population density. Thus, the established correlation between city population and urban heat island intensity (Oke, 1973) cannot be transferred to a pixel-based analysis. However, the maximum AHI (AHI_{max}) within a city can be linked to its urban heat island intensity (UHII) and is thus expected to depend on the total population of each city.

To test this hypothesis, the AHI_{max} of all German cities with a population of >100.000, as well as 100 randomly chosen smaller communities (>5000 residents), were compared to the population of the corresponding municipality (Fig. 8). Since Oke (1973) analyzed single summer temperature measurements during the day, when UHII is warmest (Schwarz et al., 2011), our annual mean temperatures result in lower heat intensities. For the three cities analyzed in both studies, this difference is on average 4.4 K (Berlin: summer day UHII of 10.0 K, annual mean surface AHI 3.7 K; Munich: summer day UHII of 7.0 K, annual mean surface AHI 4.3 K; Karlsruhe: summer day UHII of 7.0 K, annual mean surface AHI 2.9 K).

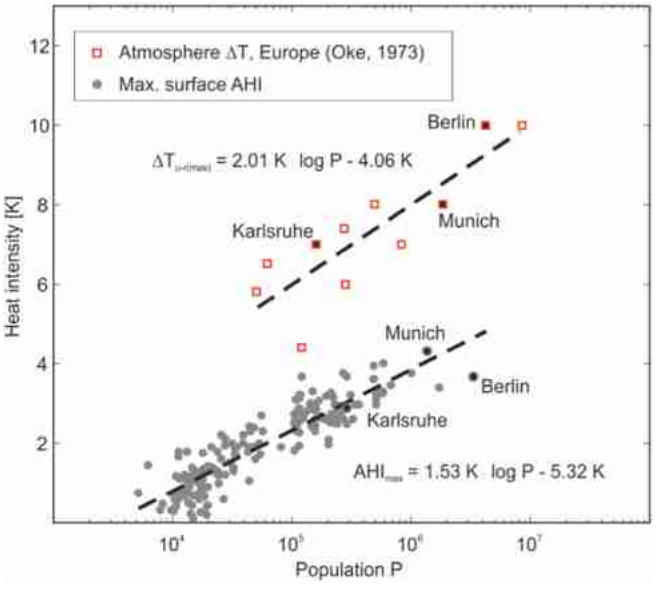

Fig. 8. Influence of population on the maximum surface AHI of a settlement.

Still, our results confirm that AHI_{max} similar to UHII can be related to population (P) and follows the model predicted by Oke (1973) even for smaller city sizes with a RMSE of 0.4 K:

$$AHI_{max} = 1.53\ K \cdot \log(P) - 5.32\ K \quad (2)$$

By extrapolating the fit, we can further assume that AHI_{max} remains positive for communities with a population of >3000. The smallest studied community, Amoeneburg located in the region of Middle Hesse, has a population of 5010 and an observed AHI_{max} of 0.74 K.

4. Summary and conclusion

This study analyzes the anthropogenic impact on recorded annual mean temperatures of three different compartments: surface air temperatures (SAT), land surface temperatures (LST), and groundwater temperatures (GWT). The anthropogenic heat intensity (AHI) is introduced as a universal parameter that represents the difference between local temperature T and median rural background temperature T_r for each analyzed measurement location (GWT and SAT) or pixel (LST), on a large, in this case countrywide, scale.

Comparing AHIs in air, surface and subsurface for the case of Germany, we found that GWTs are impacted the most by human activity. Although no measurements within cities were analyzed, determined groundwater AHI ranges from −4 K to +4 K. At the same locations, surface AHI ranges from −1 K to +1 K. However, further research is necessary to fully understand the main causes of elevated GWTs under non-urban, cultivated lands.

At the surface, main instances of anthropogenic temperature anomalies were identified. While most of the top 50 pixels with the highest AHIs in Germany are located within cities, maximum surface AHI is found over an open-pit lignite mine. Additionally, many of these top 50 pixels are located in smaller cities known for their industrial sites, hinting to the industrial sector as a significant driver of urban heat islands. Accordingly no correlation between population density and AHI could be found.

The impact of smaller settlements on temperatures was analyzed at the example of 100 randomly chosen communities (5000 to 100,000 residents). Our results indicate AHI of approximately 0.3 K for the smallest analyzed communities. However, further studies using different timescales and spatial resolutions are necessary to scrutinize the impact that smaller settlements have on ambient air, ground and groundwater temperatures.

Finally, AHIs of other regions or countries must be compared to determine spatial consistency and to reveal large scale trends. As LST is available for the whole planet, future work should also analyze a global dataset. Studying the differences in daytime and nighttime surface AHI as well as its annual variation will help to classify surface urban heat islands and thus contribute to the development of appropriate mitigation strategies.

Acknowledgment

The financial support for S. Benz from the German Research Foundation (DFG) under grant number BL 1015/4-1 and the Swiss National Science Foundation (SNF) under grant number 200021 L 144288 is gratefully acknowledged. Furthermore, we would like to thank Tanja Liesch (KIT) and Martina Maisch (LUBW) for sharing information on groundwater temperature data, and Anja Hardel and Sven Bäumer (Statistisches Bundesamt, Zensus 2011) for sharing information on the population density of Germany. Finally, we would like thank the two anonymous reviewers for their comments.

Appendix A. Supplementary data

Supplementary data to this article can be found online at http://dx.doi.org/10.1016/j.scitotenv.2017.01.139.

References

Benz, S.A., 2016. Human Impact on Groundwater Temperatures. PhD. Karlsruhe Institute of Technology, KIT.
Benz, S.A., Bayer, P., Blum, P., 2017. Global Patterns of Shallow Groundwater Temperatures. Environ. Res. Lett. (in review).
Benz, S.A., Bayer, P., Goettsche, F.M., Olesen, F.S., Blum, P., 2016. Linking surface urban heat islands with groundwater temperatures. Environ. Sci. Technol. 50, 70–78.
Benz, S.A., Bayer, P., Menberg, K., Jung, S., Blum, P., 2015. Spatial resolution of anthropogenic heat fluxes into urban aquifers. Sci. Total Environ. 524–525, 427–439.
Bowler, D.E., Buyung-Ali, L., Knight, T.M., Pullin, A.S., 2010. Urban greening to cool towns and cities: a systematic review of the empirical evidence. Landsc. Urban Plan. 97, 147–155.
Brundl, W., Hoppe, P., 1984. Advantages and disadvantages of the urban heat-island - an evaluation according to the hygro-thermic effects. Archives for Meteorology Geophysics and Bioclimatology Series B - Theoretical and Applied Climatology. 35, pp. 55–66.
Chow, W.T.L., Roth, M., 2006. Temporal dynamics of the urban heat island of Singapore. Int. J. Climatol. 26, 2243–2260.
DWD, d. Deutscher Wetterdienst, Climate Data Center (CDC). accessed 4 July 2016 at URL. ftp://ftp-cdc.dwd.de/pub/CDC/.
Dhainaut, J.F., Claessens, Y.E., Ginsburg, C., Riou, B., 2004. Unprecedented heat-related deaths during the 2003 heat wave in Paris: consequences on emergency departments. Crit. Care 8, 1–2.
Doyle, D., Hawkins, T.W., 2008. Assessing a small summer urban heat island in rural south central Pennsylvania. Geographical Bulletin - Gamma Theta Upsilon. 49, pp. 65–76.
Fallmann, J., Emeis, S., Suppan, P., 2013. Mitigation of urban heat stress -a modelling case study for the area of Stuttgart. Erde 144, 202–216.
Giannopoulou, K., Livada, I., Santamouris, M., Saliari, M., Assimakopoulos, M., Caouris, Y.G., 2011. On the characteristics of the summer urban heat island in Athens, Greece. Sustainable Cities and Society. 1, pp. 16–28.
Gioia, A., Paolini, L., Malizia, A., Oltra-Carrio, R., Sobrino, J.A., 2014. Size matters: vegetation patch size and surface temperature relationship in foothills cities of northwestern Argentina. Urban Ecosystems. 17, pp. 1161–1174.
GlobCover, 2009. Project, ESA, Université Catholique de Louvain, accessed 22 Dec 2015 at URL. http://due.esrin.esa.int/page_globcover.php.
Google Earth Engine Team, 2015. Google earth engine: a planetary-scale geospatial analysis platform. https://earthengine.google.com.
Hinkel, K.M., Nelson, F.E., Klene, A.F., Bell, J.H., 2003. The urban heat island in winter at Barrow, Alaska. Int. J. Climatol. 23, 1889–1905.
Hoffmann, P., Krueger, O., Schlünzen, K.H., 2012. A statistical model for the urban heat island and its application to a climate change scenario. Int. J. Climatol. 32, 1238–1248.
Hung, T., Uchihama, D., Ochi, S., Yasuoka, Y., 2006. Assessment with satellite data of the urban heat island effects in Asian mega cities. Int. J. Appl. Earth Obs. Geoinf. 8, 34–48.
Imhoff, M.L., Zhang, P., Wolfe, R.E., Bounoua, L., 2010. Remote sensing of the urban heat island effect across biomes in the continental USA. Remote Sens. Environ. 114, 504–513.
IPCC, Climate Change, 2013. The Physical Science Basis. Contribution of Working Group I to the Fifth Assessment Report of the Intergovernmental Panel on Climate Change. Cambridge University Press, Cambridge, United Kingdom and New York, NY, USA.
Jochner, S., Menzel, A., 2015. Urban phenological studies - past, present, future. Environ. Pollut. 203, 250–261.
Karl, T.R., Trenberth, K.E., 2003. Modern global climate change. Science 302, 1719–1723.
Kurylyk, B.L., MacQuarrie, K.T.B., McKenzie, J.M., 2014. Climate change impacts on groundwater and soil temperatures in cold and temperate regions: implications, mathematical theory, and emerging simulation tools. Earth Sci. Rev. 138, 313–334.
Li, D., Zhao, X., Li, X., 2016. Remote sensing of human beings – a perspective from nighttime light. Geo-spatial Information Science. 19, pp. 69–79.
Li, W.F., Bai, Y., Chen, Q.W., He, K., Ji, X.H., Han, C.M., 2014. Discrepant impacts of land use and land cover on urban heat islands: a case study of Shanghai, China. Ecol. Indic. 47, 171–178.
LUBW, July 2016. Jahresdatenkatalog Grundwasser. Landesanstalt für Umwelt, Messungen und Naturschutz, Baden-Württemberg, Germany accessed 28 at URL. http://193.197.158.205/servlet/is/200/.
Martin-Vide, J., Sarricolea, P., Moreno-García, M.C., 2015. On the definition of urban heat island intensity: the "rural" reference. Front. Earth Sci. 3.
Mellander, C., Lobo, J., Stolarick, K., Matheson, Z., 2015. Night-time light data: a good proxy measure for economic activity? PLoS One 10, e0139779.
Menberg, K., Bayer, P., Zosseder, K., Rumohr, S., Blum, P., 2013a. Subsurface urban heat islands in German cities. Sci. Total Environ. 442, 123–133.
Menberg, K., Blum, P., Schaffitel, A., Bayer, P., 2013b. Long-term evolution of anthropogenic heat fluxes into a subsurface urban heat island. Environ. Sci. Technol. 47, 9747–9755.
Middel, A., Häb, K., Brazel, A.J., Martin, C.A., Guhathakurta, S., 2014. Impact of urban form and design on mid-afternoon microclimate in Phoenix local climate zones. Landsc. Urban Plan. 122, 16–28.
Oke, T.R., 1973. City size and the urban heat island. Atmos. Environ. 7 (1967), 769–779.
Peng, S., Piao, S., Ciais, P., Friedlingstein, P., Ottle, C., Breon, F.M., et al., 2012. Surface urban heat island across 419 global big cities. Environ. Sci. Technol. 46, 696–703.
Perrier, F., Le Mouel, J.L., Poirier, J.P., Shnirman, M.G., 2005. Long-term climate change and surface versus underground temperature measurements in Paris. Int. J. Climatol. 25, 1619–1631.

Pongracz, R., Bartholy, J., Dezso, Z., 2010. Application of remotely sensed thermal information to urban climatology of central European cities. Phys. Chem. Earth 35, 95–99.
Rajasekar, U., Weng, Q.H., 2009. Urban heat island monitoring and analysis using a non-parametric model: a case study of Indianapolis. ISPRS J. Photogramm. Remote Sens. 64, 86–96.
Rhee, J., Park, S., Lu, Z.Y., 2014. Relationship between land cover patterns and surface temperature in urban areas. Gisci. Remote Sens. 51, 521–536.
Rotem-Mindali, O., Michael, Y., Helman, D., Lensky, I.M., 2015. The role of local land-use on the urban heat island effect of Tel Aviv as assessed from satellite remote sensing. Appl. Geogr. 56, 145–153.
Santamouris, M., 2014. On the energy impact of urban heat island and global warming on buildings. Energ. Buildings 82, 100–113.
Santamouris, M., 2015. Analyzing the heat island magnitude and characteristics in one hundred Asian and Australian cities and regions. Sci. Total Environ. 512–513, 582–598.
Schwarz, N., Lautenbach, S., Seppelt, R., 2011. Exploring indicators for quantifying surface urban heat islands of European cities with MODIS land surface temperatures. Remote Sens. Environ. 115, 3175–3186.
Schwarz, N., Schlink, U., Franck, U., Großmann, K., 2012. Relationship of land surface and air temperatures and its implications for quantifying urban heat island indicators—an application for the city of Leipzig (Germany). Ecol. Indic. 18, 693–704.
Skinner, W.R., Majorowicz, J.A., 1999. Regional climatic warming and associated twentieth century land-cover changes in north-western North America. Clim. Res. 12, 39–52.
Smerdon, J.E., Pollack, H.N., Cermak, V., Enz, J.W., Kresl, M., Safanda, J., et al., 2006. Daily, seasonal, and annual relationships between air and subsurface temperatures. J. Geophys. Res.-Atmos. 111.
Statistisches Bundesamt, Regionaldatenbank Deutschland, 2016. Statistische Ämter des Bundes und der Länder, accessed 13. September at URL. https://www.regionalstatistik.de.
Statistisches Bundesamt, Zensusdatenbank, 2011. Statistische Ämter des Bundes und der Länder, accessed 26 May 2016, at URL. https://www.zensus2011.de/SharedDocs/Aktuelles/Ergebnisse/DemografischeGrunddaten.html.
Stauffer, F., Bayer, P., Blum, P., Molina-Giraldo, N., Kinzelbach, W., 2013. Thermal Use of Shallow Groundwater.
Stegner, J., 2016. Bestimmung thermischer Materialkennwerte von Erdkabelbettungen. PhD. TU Darmstadt, Germany.
Stewart, I.D., Oke, T.R., 2012. Local climate zones for urban temperature studies. Bull. Am. Meteorol. Soc. 93, 1879–1900.
Stewart, I.D., Oke, T.R., Krayenhoff, E.S., 2014. Evaluation of the 'local climate zone' scheme using temperature observations and model simulations. Int. J. Climatol. 34, 1062–1080.
Wan, Z.M., Dozier, J., 1996. A generalized split-window algorithm for retrieving land-surface temperature from space. IEEE Trans. Geosci. Remote Sens. 34, 892–905.
Ward, K., Lauf, S., Kleinschmit, B., Endlicher, W., 2016. Heat waves and urban heat islands in Europe: a review of relevant drivers. Sci. Total Environ. 569–570, 527–539.
Weber, N., Haase, D., Franck, U., 2014. Zooming into temperature conditions in the city of Leipzig: how do urban built and green structures influence earth surface temperatures in the city? Sci. Total Environ. 496, 289–298.
Yow, D.M., 2007. Urban heat islands: observations, impacts, and adaptation. Geography Compass. 1, pp. 1227–1251.
Zhang, P., Imhoff, M.L., Wolfe, R.E., Bounoua, L., 2014. Characterizing urban heat islands of global settlements using MODIS and nighttime lights products. Can. J. Remote. Sens. 36, 185–196.
Zhibin, R., Haifeng, Z., Xingyuan, H., Dan, Z., Xingyang, Y., 2014. Estimation of the relationship between urban vegetation configuration and land surface temperature with remote sensing. J. Indian Soc. Remote Sens. 43, 89–100.